RESIDUAL STRESSES IN A TWO PHASE CONCENTRIC CYLINDER CONFIGURATION

Colpo. F, Humbert L, Botsis J.
Laboratory of Applied Mechanics and Reliability Analysis, College of Engineering, Swiss Federal Institute of Technology, Lausanne, Switzerland

ABSTRACT

Long gauge length fibre Bragg grating (FBG) sensors and a novel method, based on optical low coherence reflectometry, are used for the determination of residual strains induced in a relatively long fibre-glass reinforced cylindrical epoxy specimens after polymerisation. The fibre with the grating on its core is centrally located and surrounded by the epoxy thus, working as a reinforcement and as a sensor. The optical method allows the reconstruction of the modification of the local Bragg wavelength of the grating due to the process-induced deformation, thus providing the strain distribution along the grating length. An equivalent thermo-elastic approach, combined with the crack compliance method, is proposed to describe the residual strain field in the whole specimen after curing and post-curing processes. The modelling involves the introduction of an axial position-dependent shrinkage function S_m, whose distribution is determined from experimental data provided by the FBG. In the analysis so far, S_m is assumed independent of the radial direction. To further investigate the radial dependence of the residual stress the crack compliance method is adapted to the cylindrical geometry by measuring strains with the FBG, as a function of a radial crack. This profile can serve as an input for the evaluation of the radial dependence of S_m. In addition, these measurements may be used to deduce a) the zone of influence of the reinforcing fibre on the residual stresses and b) the effect of the presence of the mechanically induced crack on the specimen. These results show that the internal strain measurements from an embedded sensor, acting also as a reinforcing fibre can provide important information on the state of deformation and fracture behaviour of polymeric composite materials.

1 INTRODUCTION

Optical Fibre Bragg Grating (FBG) sensor and the optical low coherence reflectometry (OLCR) technique have been employed to investigate the residual strain field arising along a glass fibre included in a epoxy cylinder during curing and post curing processes. The studied specimens have a length of 40 mm and a diameter of 25 mm and the embedded fibre typically contains a 24-mm-long FBG. Mechanically, the glass fibre acts as a cylindrical elastic inclusion and locally promotes the development of residual stresses that are caused by epoxy shrinkage. The presence of a non-uniform stress field along the grating, causes a considerable modification of the FBG response. That is, for an initial uniform grating, the single Bragg peak becomes relatively broader, splits into multiple peaks and is generally accompanied with a decrease of reflectivity. The grating is said to be “chirped” and the FBG’s spectra are more complicated to interpret and cannot be directly related to strain distributions along the grating length. In this case, the FBG parameters, including grating and optical periods, are functions of the position along the fibre axis. Even if other existing techniques allow to reconstruct strain profiles from spectral amplitude measurements alone, they generally require a priori strong assumptions on the strain distribution because the phase information is not known. Alternatively, the strain profile can be determined in time domain from FBG’s impulse response. This is achieved by using a novel method developed at EPFL [1], which combines the OLCR technique and a back-scattering technique called layer-peeling. This method leads to direct reconstructions of the optical period and related strain profiles along the sensing length without any initial assumption and a spatial resolution up to 20 μm [1,2]. Assuming an

axisymmetric mode of deformation, the residual stresses into the whole specimen are properly modelled by considering a thermo-elastic approach. Based on the response of the FBG, a matrix shrinkage function S_m is introduced to describe the thermo-elastic effect. The function S_m is approximated as a polynomial function of the axial coordinate z and kept constant along the radial direction r. The results of the experiments and simulations are in good agreement with available data in the literature. The response of the FBG is also recorded for various depths of a radial crack on the cylindrical specimen. These data can be consequently used with the compliance method to deduce the level of residual stresses along the radial direction.

2 OPTICAL METHODS AND SPECIMENS FABRICATION

2.1 Optical fibre Bragg grating sensor: general working principles

A Bragg grating can be defined as a spatial modulation (or quasi periodic modulation) of the refractive index created along a desired length of the core of an optical fibre obtained by means of the two-beam interference technique or phase mask method. For an homogeneous grating inscribed into a low-birefringence single mode (SM) fibre, the FBG's reflected signal comprises a single narrow peak centred at the Bragg wavelength λ_{B0}, which is related to the product of the mean effective refractive index n_{eff} and the grating period Λ through the Bragg condition

$$\lambda_{B0} = 2n_{eff}\Lambda \tag{1}$$

The spectral response of the FBG is influenced by the environmental conditions. In particular, both strain and thermal variations in the grating region induce changes in the effective index of the fibre and the grating period, resulting in a modification of the Bragg condition. Thus, when the grating is subjected to uniform changes in strain and/or temperature all grating periods experience the same changes showed by a simple shift of the Bragg wavelength without modification of the spectrum shape. For a non-uniform variation in applied loading or temperature, the resulting Bragg wavelength becomes a function of the position z along the grating. When the experimental conditions are such that $\varepsilon_{x,y}=-\nu_f \varepsilon_z$ (ν_f is the Poisson's ratio of the fibre), assuming also constant temperature as well as neglecting all birefringence effects, the local Bragg wavelength shift $\Delta\lambda_B(z)= \lambda_B(z)- \lambda_{B0}(z)$ is related to the applied axial strain ε_z by

$$\frac{\Delta\lambda_B(z)}{\lambda_{B0}(z)} = (1 - p_e)\varepsilon_z(z) \tag{2}$$

where $p_e = \left[1 - \frac{n_{eff}^2}{2}\left((1-\nu_f)p_{12} - \nu_f p_{11}\right)\right]$ is the effective photo-elastic coefficient which can be experimentally determined and p_{11}, p_{12} are the Pockels strain-optic constants of the undisturbed fibre. The function $\lambda_{B0}(z)$ stands for a non-uniform Bragg condition at the chosen reference state.

2.2 OLCR technique to measure the FBG response

As indicated in eqn (2), the strain distribution along the grating requires the knowledge of the local Bragg wavelengths corresponding to the actual and reference states. According to the coupled-mode theory [3], light propagation through a FBG can be described by the introduction of a unique complex coupling coefficient $q(z)$ to be determined. The novel OLCR apparatus, designed at EPFL, allows a precise measurement of the FBG complex impulse response $h(t)$ (where t represents the time variable) with high precision and low noise (generally below -120 dB). The measurement principle is based on the inherent property of a broadband light source to only

interfere with a very small delayed part of itself. The incident light is sent into the reflectometer where it is split by a 3-dB coupler into two equal beams which illuminate the reference and test arms. The latter contains the FBG. In the reference arm, light is reflected by a mirror which is mounted on a translating stage. By moving the mirror, one interrogates the FBG on its overall length. Then, the total backward signal is filtered before to be recorded by a dual phase lock-in amplifier included in the detection system that simultaneously extracts the amplitude and phase of $h(t)$. Once $h(t)$ is measured, one calculates the spectral response $r(\lambda)$ of the grating by Fourier transform and the coupling coefficient $q(z)$ can be retrieved from $r(\lambda)$ using the layer peeling reconstruction algorithm. Finally, the local Bragg wavelength $\lambda_B(z)$ is obtained by the derivative of the phase $\phi(z)$ of the complex coupling coefficient through

$$\lambda_B(z) = 2n_{eff}\Lambda_d\left(1+\frac{\Lambda_d}{2\pi}\frac{d\phi(z)}{dz}\right)^{-1} \tag{3}$$

where Λ_d is the design grating period.

2.3 Specimen preparation

Epoxy cylinders with an external radius and length of 12.5 mm and 40 mm, respectively, are manufactured. The resulting cylindrical configuration is simpler to use in numerical simulations and also allows the results to be compared with existing analytical models. Each specimen contains a standard optical glass fibre of 0.125 mm in diameter, centrally embedded along its axial direction as depicted in Fig. 1. Also presented in Fig. 1 is the considered system of coordinates, the z axis corresponding to the fibre axis. The optical fibre, supplied by Bragg Photonics, is equipped with a FBG of 24 mm in length, whose positioning is given in Fig. 1. Before positioning the fibre in the mould and pre-straining it to ensure a correct alignment along the z direction, its acrylate coating is stripped along the entire embedded length (L=40 mm) using a sulphuric acid bath. The stripped surface is also cleaned by means of successive baths in ethylic alcohol to assure clean interface conditions. To prepare the epoxy, an established standard protocol is followed that uses a mixture of DER 330, DER 732 Dow Epoxy resins and DEH 26 curing agent in respective weight proportions of 70:30:10. Once the polymerization process is completed at room temperature, after 24 hours, the specimen is removed from the mould and placed in an oven for the post curing at 60° for 9 hours. Then, it is left to cool inside the oven until the room temperature is reached. Using standard test methods, Young's modulus and Poisson's ratio of the epoxy are found to be 2.3 GPa and 0.38, respectively. For the glass fibre, these parameters are 72 GPa and 0.17, directly provided by the manufacturer. When the specimen preparation is completed, a precise measurement of both the length and position of the grating with reference to one end of the specimen is carried out using the OLCR apparatus.

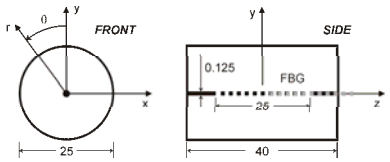

Figure 1: Schematic of the cylindrical specimen. The location of the grating is also shown when it is fully (dark line) and partially (grey line) embedded. (Dimensions are in mm).

2.4 Experimental results

As expected, the experiments indicate that the epoxy matrix material undergoes substantial shrinkage during curing and post curing processes. This effect is highlights by the analysis of the reflected FBG spectra obtained for three important steps of the specimen preparation: before embedding, two hours after curing and two hours after post curing. From the experimental results, it appears that the specimen sustains substantial non-uniform compressive strain during the fabrication, shown by the shape and position of the resulting reflected spectra. The maximum shift of the Bragg wavelength peak provides an idea of the maximum value of the deformation applied to the grating whereas the distribution of the reflected wavelengths gives information on the non uniformity of the strain profile applied along its length. It is important to notice the shape of the strain profile, with a maximum compressive strain of –2000 με and –6000 με at the centre, after curing and post curing process respectively. The same strain values are found for other experiments and attest the reproducibility of the tests. In addition, the complete strain distribution along the entire length of the embedded optical fibre core has been experimentally determined, since the FBG can be precisely located in different positions (from the centre to the outside) along the main axis of symmetry of the cylinder (see Fig 1). Particularly, the grating has been located in such way that two third of the grating length remain in the specimen and one third in the outside. However, due to the grating length, the measured strain distributions can be partially superimposed along the axial direction with those obtained by the other experiences, providing in this way another comparison and an ulterior verification on the results previously obtained. All the results are summarized on the Fig. 2.

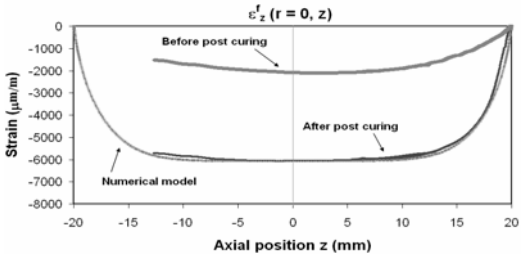

Figure 2 : Axial strain distribution measured before and after post curing. The later is compared with the numerical model.

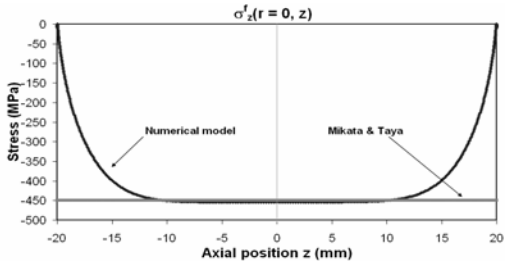

Figure 3: Simulation of the axial stress distribution along the fibre. Also presented is the axial stress given by the model of Mikata and Taya.

3 NUMERICAL SIMULATIONS

An axisymmetric finite element (FE) model is used to determine the residual stress state in the specimen. The FE calculations are performed with the commercial ABAQUS code. The specimen is considered as a cylindrical fibre-reinforced composite consisting of two concentric cylinders (two material sub-domains) described by the cylindrical coordinate system (r,θ,z). The fibre is the central cylinder of radius r_f=0.0625 mm. The matrix domain corresponds to the annulus of inner radius r_f and outer radius r_m=12.5 mm. The fibre and the matrix materials are assumed to be homogeneous and isotropic. Moreover, perfect interface conditions are considered between the two material phases. To model the matrix volumetric shrinkage effect, the problem is considered analogous to a thermo-elastic one. We also consider the elastic properties of the materials to be independent of temperature and not to change as the degree of cure advance during post-curing. As a consequence, the only residual stresses are those associated with curing shrinkage of the epoxy when the system returns to room temperature. A matrix shrinkage function S_m is then introduced in place of the term $\alpha\Delta T(r,\theta,z)$ in the thermo-elastic stress-strain relations, where α is the coefficient of thermal expansion (CTE) of the material and $T(r,\theta,z)$ is the distributed temperature inside the body. Due to the axial symmetry, the problem can be considered as two-dimensional and only the *rz*-plane (Fig. 1) needs to be meshed. Along the longitudinal and transverse directions, the matrix

domain is discretized into 200×100 elements. For the fibre, 200×30 elements are used. The mesh is constructed with parabolic axisymmetric elements and is refined towards the ends and at the fibre–matrix interface to accommodate strong variations of the field quantities.
Assuming no radial evolution the function S_m is expressed in the following form

$$S_m(z) = a\left(\frac{z}{20}\right)^4 + b\left(\frac{z}{20}\right)^2 + c \tag{4}$$

where *a, b* and *c* are constant parameters to be determined. Inserting expression (4) in the finite element model, the coefficients *a, b* and *c* can be determined using a minimization procedure between the calculated and measured strain along the grating. The simulated strain distribution along the fibre is presented in Fig. 2 and, as expected, it correctly matches the experimental measurements. Also given in Fig. 3 is the corresponding axial stress evolution along the specimen length. The present results are compared with the theoretical predictions of the model of Mikata and Taya [4] when an explicit close form solution exists for one fibre embedded in an infinite matrix. The comparison of the calculated axial stress profile along the fibre and the prediction of the model in [4] is given in Fig. 3. Note here the good agreement between the two models at the centre of the specimen. Another verification has been done to check the results given by the FE simulations. After the post cure treatment the deformed shape of a cylindrical specimen is reconstructed using a Coordinate Measuring Machine (CMM) with a resolution of 1 μm and is compared with the calculated one obtained by FE predictions. As shown in Fig. 4, even if some differences (over all at the ends of the specimen) are present due to the simplified assumption in defining (4) (i.e. S_m is considered at this phase independent of the radial direction) the simulated data are in good agreement with the measured ones.

4 RADIAL DEPENDENCE OF RESIDUAL STRESSES

The results presented in the preceding paragraphs are based on an axial dependence of the S_m function only. Although the results are good, it is necessary to introduce the r-dependency in the S_m function for a complete characterization of the residual stresses in the epoxy cylinder. Since the strain distribution along the FBG does not provide such information, one may introduce relevant theoretical r-dependent distribution [4] in the experimentally derived function S_m and compare the experimental results with those of the model. One method to extract experimental data on the residual stresses along the radial direction, using the response of the FBG, and compare the models is described below.
Taking inspiration from experiments based on the crack compliance method to provide data on the residual stress distribution [5,6], the series expansion method is adapted to the cylindrical geometry and a series of circular cracks (notches) are machined, in the middle of the cylinder, in the radial direction and perpendicular to the FBG grating as shown in the insert of Fig. 5. In this way the residual stress profile in the radial direction at a given z can be obtained. To achieve this objective, the unknown residual stresses are written as a series expansion

$$\sigma_z(r) = \sigma_0(r) = \sum_{i=0}^{n} A_i P_i(r) \tag{5}$$

where A_i are unknown coefficients and P_i are polynomials. Then the strain that would be measured at the strain location (in this case at the centre of the specimen where is placed the FBG) is

calculated for each P_i. These strains are usually indicated as compliance C_i. Using superposition, one can write the strains for the stresses given by eqn (5) as

$$\varepsilon_0(a_k) = \varepsilon_0(a_k) = \sum_{i=0}^{n} A_i C_i(a_k) \tag{6}$$

To obtain the coefficients A_i, a least-squares fit is performed between the measured strains and those given by the eqn (6) and, hence, the stresses from eqn (5).
The experimental values of strains can be directly calculated from the response of the FBG as a function of mechanically introduced cracks of increasing lengths. Typical data are shown in Fig. 5 where the local Bragg wavelength and thus, the strain is plotted as a function of the axial coordinate z, for different crack depths a. The results in Fig. 5 demonstrate that for crack depths of about 11 mm, the strain distribution along the FBG remains practically unchanged. For longer crack depths, however, a significant effect on the strain on the FBG is measured. Interestingly, the onset of changes on the residual strain due to the presence of the fibre corresponds to a distance of about 4 FBG diameters from the center of the cylinder.
Using data from such measurements, at different crack lengths, the axial residual strains on the FBG and radial stresses in the epoxy matrix, as a function of the cylinder's radius can be obtained.
The residual stress distribution along the radial direction can be used to check the predictions of the equivalent thermoelastic model under various forms of the function S_m.

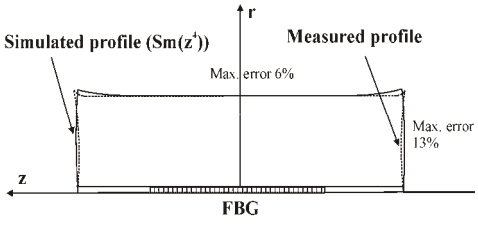

Figure 4: Comparison between the simulated and cylindrical profile and that measured with the Coordinate Measuring Machine.

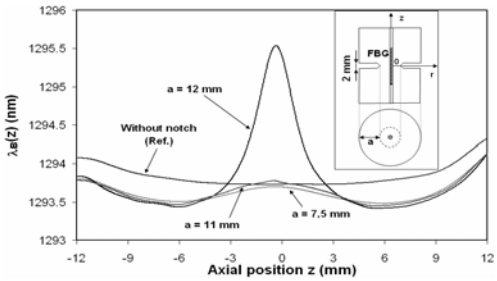

Figure 5: Plot of the measured local Bragg wavelength distribution as a function of the axial coordinate z for different notch depths a. The strain profile along the fibre is the same since the reference Bragg wavelength is constant.

5 REFERENCES

[1] Giaccari P. *Fibre Bragg grating characterisation by optical low coherence reflectometry and sensing applications.* Ph.D. Thesis n°2726, EPFL 2003.

[2] Giaccari P., Limberger H.G. and Salathé R.P. *Local coupling-coefficient characterization in fibre Bragg gratings.* Optics Letters 2003; 28(8):598-600.

[3] Snyder A.W., Love J.D. *Optical Waveguide Theory,* Chapman & Hall,1983.

[4] Mikata Y., Taya M. *Stress field in a coated continuous fibre composite subject to thermo-mechanical loadings.* Journal of Composite Material, 1985;19:554-579.

[5] Prime M.B. *Measuring residual stress and the resulting stress intensity factor in Compact Tension specimen.* Fatigue Frac. Engng. Mater. Struct. 22,:195-204, 1999.

[6] Finnie I., Cheng W. *A summary of past contribution on residual stresses.* Material Science Forum; 404-407:509-514,2002.